DOI: 10.1590/2317-4889201720170033

ARTICLE

Protracted deformation during cooling of the Paleoproterozoic arc system as constrained by $^{40}Ar/^{39}Ar$ ages of muscovite from brittle faults: the Transamazonan Bacajá Terrane, Brazil

Deformação prolongada durante o resfriamento de um arco paleoproterozoico registrado por idades $^{40}Ar/^{39}Ar$ em muscuvita de falhas rúpteis: o Terreno transamazônico Bacajá, Brazil

Edimar Perico[1], Carlos Eduardo de Mesquita Barros[2]*, Fernando Mancini[2], Sidnei Pires Rostirolla[4]

ABSTRACT: In the Paleoproterozoic Transamazonas Province, synkinematic granitogenesis has taken place synchronously with compressive tectonic stress. The synkinematic character of the granites is marked by their WNW elongate shape, and by the presence of pervasive and concordant synmagmatic foliation. Ductile shear zones are concordant to the previous regional WNW structures, and tend to be accommodated along contacts between Rhyacian synkinematic granitoids and both Archean orthogneisses and Siderian metabasites. Locally phyllonitic shear zones and brittle-ductile shear zones with cataclasites are oriented subparallel to the preexisting ductile foliation. Late orogenic brittle faults N30E-trending strike-slip faults are either sinistral or destral. $^{40}Ar/^{39}Ar$ dating of muscovite developed on fault planes gave ages of 1977 ± 8 Ma and 1968 ± 11 Ma. Structural and geochronological data from rocks of the Transamazonas Province permit to conclude that most mylonites and brittle structures were controlled by preexisting structures such as geological contacts and petrographic facies boundaries. Compressive tectonic stress would have initiated at ca. 2100 Ma, since the former magmatic arc (Bacajaí complex), still present at 2070 Ma when syntectonic granites were emplaced and remained until 1975 Ma after granite plutonism and regional cooling.

KEYWORDS: Synkinematic granites; shear zones; structural anisotropy; tectonic reactivation.

RESUMO: *Na Província Transamazonas, de idade paleoproterozoica, a granitogênese sintectônica ocorreu concomitantemente a esforços tectônicos compressivos. O caráter sintectônico dos granitos é marcado pela forma alongada dos plútons na direção WNW e pela presença de foliação sinmagmática pervasiva e concordante com aquela direção. Zoas de cisalhamento dúctil são concordantes às estruturas WNW regionais anteriores e tendem a ser acomodadas ao longo dos contatos entre granitos sintectônicos riacianos, aortognaisses arqueanos e a rochas metabásicas siderianas. Localmente, zonas de cisalhamento filoníticas e zonas de cisalhamento rúptil-dúctil com cataclasitos são subparalelas à foliação dúctil pré-existente. Falhas rúpteis tardi-orogênicas de direção N30E são sinistrais e destrais. Datações $^{40}Ar/^{39}Ar$ em muscovita desenvolvida em planos de falhas forneceram idades de 1977±8 Ma e 1968±11 Ma. Dados estruturais e geocronológicos de rochas da Província Transamazonas permitem concluir que a maioria dos milonitos a estruturas rúpteis foi controlada por estruturas pré-existentes, tais como contatos geológicos e limites de fácies petrográficas. Esforços tectônicos compressionais teriam sido iniciados em 2100 Ma durante a formação de um arco magmático precursor (Complexo Bacajaí), e se mantiveram até 2070 Ma quando granitos sintectônicos se colocaram. Esforços compressionais residuais permaneceram atuantes até 1975 Ma após a granitogênese e resfriamento regional.*

PALAVRAS-CHAVE: *granitos sintectônicos; zonas de cisalhamento; anisotropia estrutural; reativação tectônica.*

[1]Post-Graduate Program in Geology, Universidade Federal do Paraná – UFPR, Curitiba (PR), Brasil. *E-mail: ediperico@yahoo.com.br*

[2]Geology Department, Universidade Federal do Paraná – UFPR, Curitiba (PR), Brasil. *E-mails: cadubarros@ufpr.br; ferman@ufpr.br*

[4]Rosneft, Rio de Janeiro (RJ), Brasil. *E-mail: sidneiprostirolla@gmail.com*

*Corresponding author

Manuscript ID: 20170033. **Received on:** 03/14/2017. **Approved on:** 08/08/2017.

INTRODUCTION

Synkinematic granite bodies show elongated shapes concordant with the regional structural pattern and microstructural evidence of emplacement during tectonic stress field (e.g., Paterson *et al.* 1991, Miller & Paterson 1994). Mechanisms that could give rise to high temperature magmatic structures (Vigneresse *et al.* 1996, Barbey *et al.* 2008, Barbey 2009) are related to the increase in crystallization rates within the magmatic chamber. Once a critical rheological threshold is reached (Arzi 1978), the magmatic chamber obtains a viscosity similar to that of a solid, and ductile deformation structures can be formed in material that has not completely crystallized. Under these conditions, deformation is progressive and controlled by a decreasing temperature regime. The foliation that develops during crystallization is penetrative within magmatic chambers and tends to be homogenous at outcrop scale (Paterson *et al.* 1991). The formation of bodies, their internal structures and the preferred orientations of minerals constitute potential anisotropies where shear zones or faults might develop (Vauchez *et al.* 1998).

Differences in thermal gradients control the strength of different materials, with increase in resistance being directly linked to the age of the lithosphere (Vauchez *et al.* 1998). Vauchez *et al.* (1998) consider colder cratons to be more rigid than younger orogenic provinces that are dominated by higher temperature regimes. Combined rheological heterogeneity and mechanical anisotropy are fundamental factors in the deformation of continents. As an example, Vauchez *et al.* (1998) and Corrêa-Gomes *et al.* (2005) present the São Francisco Craton and the Ribeira Belt, where several regional strike-slip shear zones have preferentially developed on boundaries of cratonic provinces.

Tectonic reactivation has been discussed over many decades (Holdsworth *et al.* 1997, Vauchez *et al.* 1998, Ranalli 2000), particularly the control of preexisting basement structures (Pinheiro & Holdsworth 1997, Brown *et al.* 1999; Bailey *et al.* 2005, Marshak *et al.* 2006). Understanding the reactivation of structures can be very useful for prospecting ore deposits and to identify hydrocarbon potential of sedimentary basins (Bumby *et al.* 2001, Rostirolla *et al.* 2001, Mansy *et al.* 2003, Korme *et al.* 2004, Corrêa-Gomes *et al.* 2005).

The magmatic rocks of the Bacajá Terrane have been studied by several authors (João *et al.* 1987, Faraco *et al.* 2005, Vasquez *et al.* 2005, Barros *et al.* 2007) who describe belts of metavolcanics and concordant elongate granitic bodies. There are also shear zones in the region that have formed after complete magma crystallization. The present article discusses the nature and time of stress fields during the Transamazonian orogeny and the influence of preexisting structural anisotropy during the formation of ductile and brittle shear zones.

METHODS

This study is based on the recognition of the main structural trends with regards to structures of the Amazon Basin basement of the Bacajá domain (Fig.1), as revealed by multiscale analysis through digitalized SRTM elevation models, structural analyses on outcrops and thin sections, and geochronological data. The analysis of digitalized SRTM elevation models, acquired from the USGS site (http://eros.usgs.gov, August 2007), was done through the use of ESRI® ArcMap™ 8.3 software, aided by geological, hydrographic and other maps available in the literature.

Fieldwork in the Bacajá Terrane was done on outcrops along the Transamazônica road and also across the vicinal roads. These latter are oriented N-S direction, almost perpendicular to the regional structural trend. Thin section studies allowed us to understand the rheological conditions, mechanisms of recrystallization and to estimate the temperatures at which the granitoids of the Bacajá Terrane were deformed.

Muscovite crystals collected from brittle faults were dated using the $^{40}Ar/^{39}Ar$ method. This analysis was undertaken at the UQ-AGES Laboratory at the University of Queensland (Australia). After a period of irradiation and decay, the samples were analyzed by $^{40}Ar/^{39}Ar$ heating via laser. Before the analysis, the grains were subjected to vacuum and 200ºC temperatures for 12 hours. Each sample was gradually heated with a continuous wave Ar ion laser with an unfocused 2mm wide beam. The gas liberated by this process was cleaned by a cryo-cooled system (at T = -125ºC) and two collectors. It was then analyzed for Ar isotopes in a MAP215-50 mass spectrometer equipped with a C-50 SAEZ Zr-V-Fe collector.

GEOLOGICAL SETTING

In South America, Paleoproterozoic terranes are widely distributed throughout the Amazon Craton (Santos *et al.* 2000, Tassinari & Macambira 2004), along its southeastern portion (João *et al.* 1987, Vasquez *et al.* 2008, Macambira *et al.* 2009), through the southern extent of the Amazon Basin, and also across its north and northeastern domains, running from Amapá up to Surinam, French Guyana and Guyana (Santos *et al.* 2000, Avelar *et al.* 2003, Delor *et al.* 2003, Rosa-Costa *et al.* 2006). In this work we focus on the Bacajá Terrane (Fig. 1), which is situated in the southeastern part of the Amazon Craton, between the Carajás Archean Province and the Amazon Basin (Santos 2003, Vasquez & Rosa-Costa 2008). Its evolution is linked to crustal growth and formation of synkinematic granites (João *et al.* 1987, Barros *et al.* 2007).

According to Cordani *et al.* (1979), the Precambrian rocks of the Amazon Craton developed three mobile belts

running NW-SE around a central region made up of older rocks (Fig. 1). The Amazon Craton is composed of an Archean nuclei, mobile belts (Maroni-Itacaiúnas, Parima-Tapajós, Rio Negro-Juruena, Cachimbo Traíra, Rondoniano, Paraguai-Araguaia), NE-SW oriented shear zones, volcano-plutonic domains and a Proterozoic sedimentary cover. Noteworthy events include episodes of metamorphism (Jari-Falsino/K'Mudku, Nickerie, Orinoquense), the formation of the Amazon sineclysis and its structural arches (Lima *et al.* 2005, Cordani *et al.* 2010).

Immediately to the north of the Archean nucleus at Carajás Mining Province is the Tranzamazonas (also named Maroni-Itacaiúnas) mobile belt (2200 Ma–1900 Ma), which is oriented WNW-ESE and cut by NE-trending structures (Santos *et al.* 2000, Tassinari & Macambira 2004). The WNW-ESE regional structural trend is very well marked on aerogeophysical data (Faraco *et al.* 2005, Perico 2010, Carneiro *et al.* 2012).

The study area is located in the Maroni-Itacaiúnas Province (Transamazonas Province), which evolved during the Paleoproterozoic. Geochronological studies have revealed Archean fragments (the Aruanã Complex), 2.3 Ga Paleoproterozoic metabasites (Itatá Formation), deformed granitoids of 2.2 to 2.1 Ga representing the early accretion and recycling of Archean rocks (Bacajaí and Arapari suites), and the foliated granitoids of the João-Jorge suite, dated at 2.07 Ga (Santos *et al.* 2000, Faraco *et al.* 2005, Vasquez *et al.* 2008, Macambira *et al.* 2009). South of Transamazonas province, the largest Archean craton nuclei is represented by the Carajás Province (Santos *et al.* 2000).

Earlier studies developed in this region pointed out the complex evolution of orogenic domains controlled by granites that were emplaced during the course of tectonic compression (João *et al.* 1987). Several later studies were undertaken at the regional level (Faraco *et al.* 2005, Vasquez *et al.* 2005) in what was then called the Bacajá Terrane (Santos, 2003). Regional lithologic layering is marked by the presence of kilometer-long lenses of metabasites oriented along the WNW direction parallel to the elongate granite bodies composed of differently foliated rocks. Barros *et al.* (2007) identified different structures in granitoids, many of which were interpreted to have formed in the magmatic stage, suggesting that granite emplacement was synchronous to regional compressive tectonic stress.

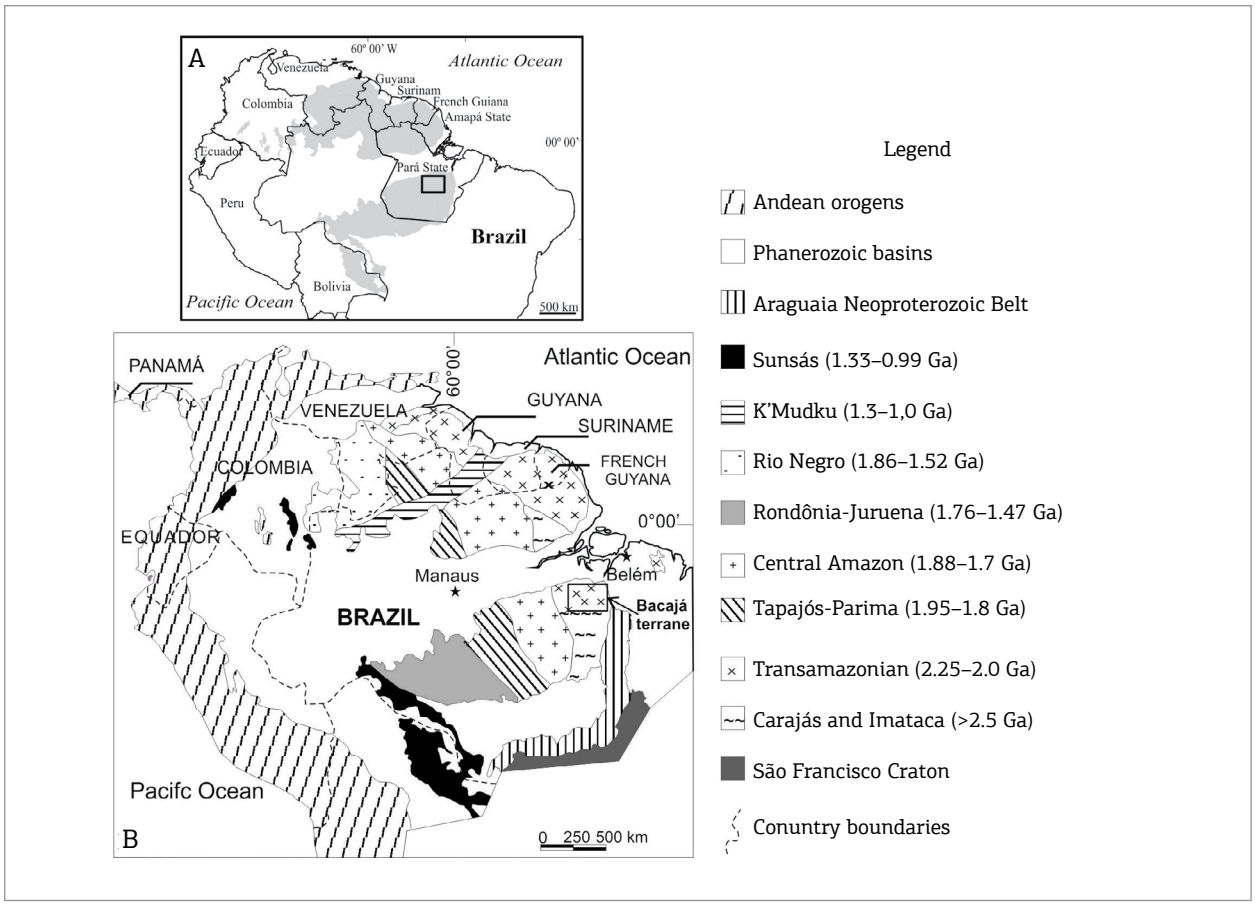

Figure 1. Geochronological provinces of the Amazon Craton (cf. Tassinari & Macambira 2004). The rectangle shows the study area.

STRUCTURAL GEOLOGY

Paleoproterozoic metabasic rocks

Metabasites and amphibolites compose a N70W-striking belt having dozens of kilometers long and few hundred meters wide (Fig. 2). These rocks belong to the Itatá Formation of the Três Palmeiras Group (João *et al.* 1987, Vasquez & Rosa-Costa 2008) and are limited to the north and south by granitic bodies. Along the contacts between granitic plutons, the metabasic rocks display a strong N78/75SW foliation marked by preferred orientation of plagioclase and olive green amphibole. Where this foliation is not present, the metabasites show a massive structure and blastophitic texture. Brittle structures are represented by NNE-SSW, NE-SW and NW-SE fractures. En-echelon N45E fractures indicating dextral movement were observed near the contacts to granites.

Paleoproterozoic granitoids

The mesoscale structures are primary igneous layering, magmatic foliation with solid-state component, ductile shear zones, phyllonites, britlle-ductile shear zones, brittle faults and fractures. The schematic structural map (Fig. 2) shows the areas where the main structural features have been described. Among these structures, the first three are similar to those described by Barros *et al.* (2007).

Igneous layering

The term "layering", sensu Barbey (2009), refers to rhythmic alternation of layers of different compositions or grain sizes. Layering is commonly observed in the study area, and is defined by the rhythmic alternation of quartz-feldspathic and ferromagnesian levels (Fig. 3a). Sometimes the layering is marked by the alternation of fine-to medium-grained levels with coarse-grained domains. Pegmatite or aplite veins are locally found parallel to the layering, emphasizing the rhythmic alternation. In the granitoids from the Bacajá Terrane, magmatic layering shows subvertical and subhorizontal dips. In the first case, the strike varies from E-W to N70W. In the second case, the layering is generally affected by gentle WNW-trending folds with subvertical axial planes.

Quartzo-feldspathic veins

Quartzo-feldspathic veins and their host granitoids commonly present magmatic foliation. Earlier veins may be folded and more strongly foliated than the later veins where foliation is generally weakly developed. Examples of these features can be found in many outcrops in the Bacajaí, Arapari and João Jorge intrusive suites. At least three phases of quartz-feldspathic veins have been identified, many of which have been affected by dextral faults running N80E and by en-echelon sinistral fractures striking N45E.

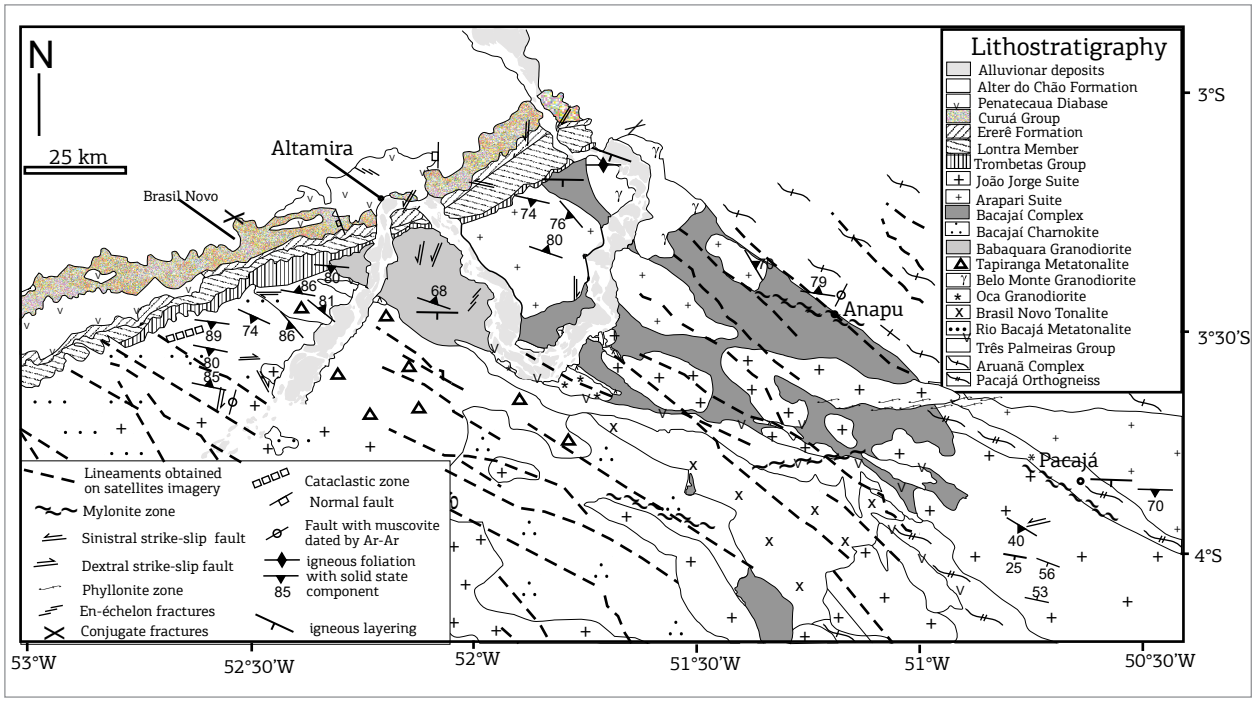

Figure 2. Schematic geological map of the Bacajá Terrane showing the main structures and the location of the muscovite-bearing faults dated by the Ar-Ar method.

Magmatic foliation with solid-state component (Sn+1)

When compressional tectonic stress is imposed during crystallization of magmas, the final structural pattern may be difficult to distinguish from metamorphic gneissic foliation observed in quartzo-feldspathic rocks. Criteria used to clarify these situations have been proposed by several authors (Paterson *et al.* 1989, 1998, Gower 1993, Miller & Paterson 1994, Pons *et al.* 1995, 2006, Barbey *et al.* 2008), and include the preferred orientation of undeformed crystals (mainly quartz), laterally homogenous ductile foliation surrounding xenolithes, presence of late magmatic shear zones that collect residual melts, coexistence of early foliated pegmatites with late weakly- or non-foliated pegmatites, and tectonically-controlled symplectites.

In cases where magmas are progressively deformed during cooling, the resulting fabric vary from preferred orientation of weakly deformed crystals to strongly flattened rocks showing gneissic aspect (Barros *et al.* 2001, Pawley & Collins 2002). Magmatic foliation with a solid-state component is found in granites throughout the region. N80W to N60W foliation in these cases is moderate to weak and defined by the preferred orientation of ferromagnesian minerals, feldspars and quartz. Outcrops and thin section analyses of granitoids throughout the region permit to suggest that quartz was deformed mainly by flattening. Quartz deformation varies from weak to strong, and is marked by the presence of weakly elongated aggregates of subgrains and new grains. Elongate mafic enclaves are parallel to foliation observed in the host granitoids suggesting that deformation, magma crystallization and development of foliation Sn+1 were synchronous. In general, magmatic foliation with solid state components (Sn+1) is subparallel to the primary subvertical layering. In rocks with porphyritic texture, we find a preferential orientation of the euhedral microcline phenocrysts. Some isolated phenocrysts are disposed obliquely or perpendicularly to the foliation, indicating crystal rotation in the presence of liquid. Locally, foliation detours around amphibolite xenolithes. This demonstrates a large viscosity difference between the xenolith and the partially crystallized acid magma.

Figure 3. Structures present in Paleoproterozoic granitoids from the Bacajá Terrane, Amazon Craton. (A) Igneous layering; (B) photomicrography (polarized light) of weak magmatic foliation; (C) magmatic foliation with solid state component (protomylonite); (D) photomicrography (polarized light) of granite mylonite.

In weakly foliated granitoids, the quartz is fine-to medium-grained, has weak to moderate preferred orientation and show strong undulose extinction, subgrains and new grains (Fig.3b). Sutured contacts between new grains of quartz suggest high temperature recrystallization controlled by grain boundary migration. The microcline crystals are inequigranular, fine and medium, occasionally large, anhedral and subhedral, showing weak preferential orientation and sometimes flame perthites. Microcline shows moderate wavy extinction and well-developed crossed twins, while plagioclase crystals are inequigranular, fine and medium, occasionally large, anhedral and subhedral and have weak to moderate preferred orientation. Plagioclase also shows undulose extinction, kink bands and small fractures.

The biotite crystals are fine, anhedral and subhedral and display moderate preferred orientation. Biotite crystals also occur as elongated clots parallel to the foliation. Recrystallization of biotite produced thin levels of new grains disposed close to coarse and deformed crystals. Symplectites of biotite and amphiboles formed by stress-controlled corrosion of faces parallel to the foliation can be observed. Barros *et al*. (2007) have considered this texture as the result of tectonic stress on non-completely consolidated magma.

Ductile shear zones

The shear zones are decimeter to meterwide, and in general NW-SE trending with a subvertical orientation concordant with the regional structures (Fig.2). The rocks within the shear zones are gray and more fine-grained than the host rock. In protomylonites (Fig. 3c), quartz crystals form aggregates of new grains and subgrains with strong preferred orientation and anastomosed aspect, especially around prophyroclasts. In some elongated quartz aggregates, subgrain boundaries are oriented oblique to the foliation. The microcline is fine-to coarse-grained, anhedral and subhedral and locally augen-shaped. Microcline has a preferred orientation, flame perthites and shows recrystallized margins with fine new grains. Undulose extinction varies from weak to strong, evolving towards subgrains and micro-faults. The plagioclase crystals are fine- to coarse-grained, anhedral and subhedral and display a good preferential orientation. Biotite forms anastomosed levels and shows recrystallization along its edges, kink bands and fish-shape.

West of Altamira a 50m wide mylonite/ultramylonite is found. Themylonites are fine-grained and dark gray and has a N45W/subvertical orientation. Mineral lineations associated with this plane have a plunge of 05/125. Quartz is fine, anhedral, has irregular contacts, and shows undulose extinction, subgrains and neoblasts. Quartz forms the rock matrix in oriented and anastomosed fine levels. The microcline is fine to coarse-grained, anhedral and shows recrystallized edges, irregular contacts and augen-shaped forms, strong undulose extinction and flame perthites. The new fine grains of microcline, plagioclase and quartz form the matrix. Some plagioclase crystals are augen-shaped and recrystallization along the edges has produced fine new grains (Fig. 3d).

South of Anapu (Fig. 2), meter-wide WNW-trending mylonite zones developed along the contacts between the orthogneisses of the Aruanã Complex and the syntectonic foliated granitoids of the Bacajaí and Arapari suites.

Phyllonites

Between Bom Jardim and Anapu villages, a kilometer long and decameter wide N80E/84SE shear zone crosscuts the granitoids (Fig. 2). This shear zone is located along the contact between the Pacajá orthogneisses and the granitoids of the João Jorge suite. The most striking feature of this structure is the presence of muscovite-chlorite(?)-quartz-rich phyllonites (Fig. 4a). 0.5 to 1 meter-wide veins of quartz can be observed in this shear zone.

Brittle-ductile shear zones

Locally, foliated granitoids were affected by decimeter- to meter-wide brittle-ductile faults striking N60W with subvertical dips. In these cases, intense deformation has reduced the size of the grains and altered the color of the rocks to a dark gray. These cataclasites contain up to three centimeters wide quartz veins that may or may not have formed at the same time as the cataclasites.

Under the microscope, the cataclasites are characterized by the presence of strongly strained inequigranular anhedral quartz. The quartz crystals are fine-grained and show strong undulose extinction, deformation lamella and subgrains. Crystal showing irregular forms and sizes varying from very fine to coarse suggest that cataclastic flow with crystal fragmentation was the dominant formation mechanism. Fine veins of quartz or epidote occasionally fill faults and fractures. Microcline has well developed perthites, strong undulose extinction and microfractures and microfaults. Plagioclase crystals are fine- to coarse-grained and display slightly curved twinned crystals, microfaults and undulose extinction. In the most intensely deformed zones, anhedral crystals make up the largest part of the cataclastic matrix (Figs. 4b and 4c), which is composed of angular crystals of varying sizes. In the domains where intense deformation has taken place, epidote and opaque minerals are commonly found. Near the shear zone, the feldspar is fractured, shows microfaults and is cut by epidote veins.

Brittle faults

The faults that affect the granitoids have few tens of meter wide and kilometers length. The fault planes show striations and steps (Figs. 4d, 4e and 4f), en-echelon fractures, sigmoidal brittle structures and vein displacements. Near Anapu N30W/81NE brittle faults and 142/24 striations were observed. These features attest to the strike-slip character of these faults. Some faults have decimeter to meter-sized steps (megasteps) indicating sinistral sense. In this outcrop, there are also N33E/87SE oriented faults

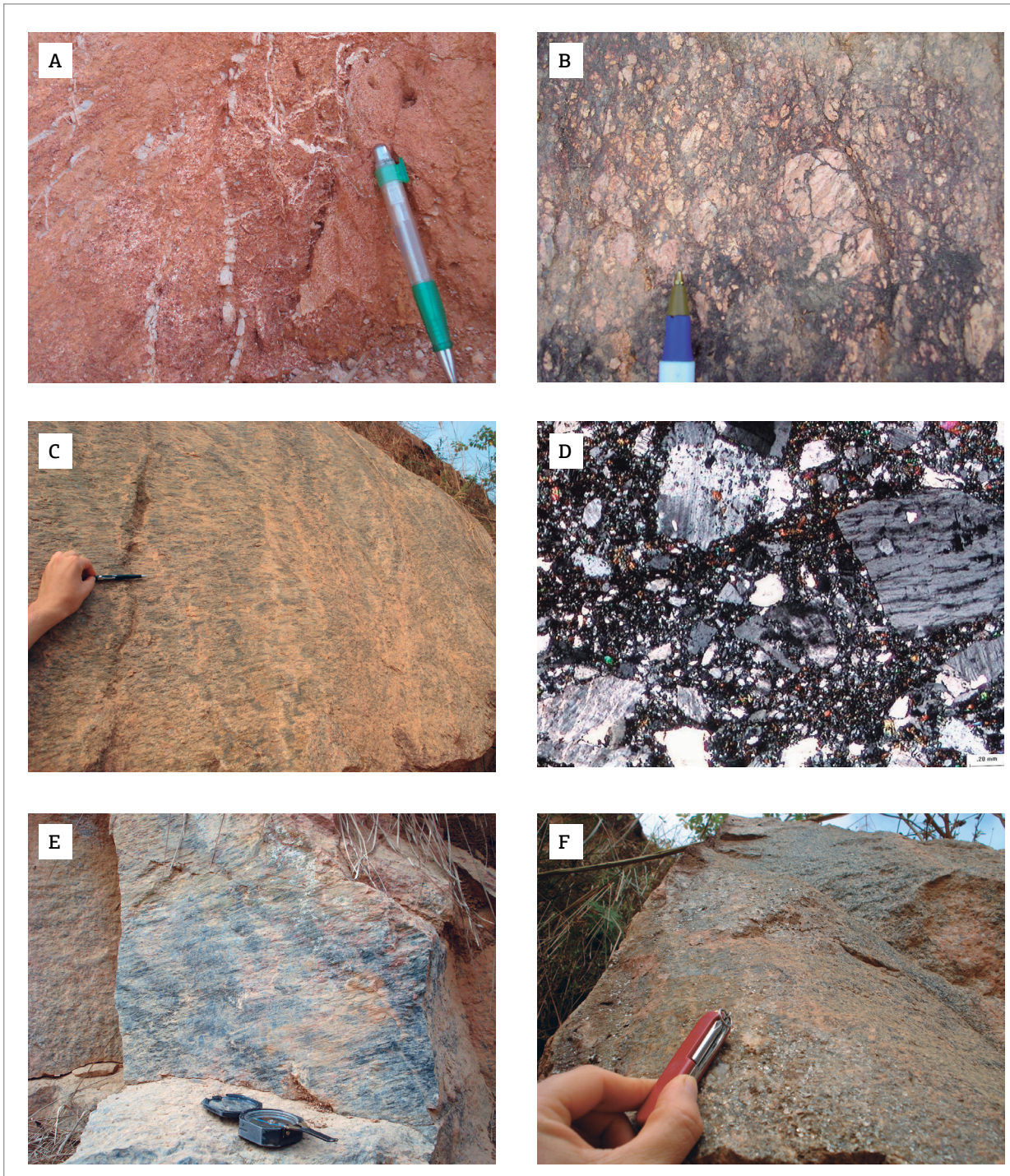

Figure 4. Structures of Paleoproterozoic granitoids from the Bacajá Terrane, Amazon Craton. (A) Phyllonite zone; (B) Cataclastic zone; (C) Photomicrography (polarized light) of cataclasite; (D) Fault plane with megasteps indicating destral sense; (E) and (F) N30E fault plane with gently plunging striations and muscovite crystals.

with kinematic indicators showing sinistral movement. Muscovite crystals formed on this plane were collected for $^{40}Ar/^{39}Ar$ dating (Fig. 4f).

Crosscutting relationships suggest that the N33E fault could be formed after the N30W faults mentioned above. In many situations, the principal direction of the fractures and the kinematic indicators correspond to the Y, R and R fractures of Riedel's model. The orientation of the N33E/87SE faults is almost parallel to the maximum principal stress direction (N30E) of a tectonic stress field that would have been present since the magmatic arc growth. In the outcrop where phyllonites are found (PMI-11), three main families of later faults have been identified. Here, the repeated patterns and angular relationships of the fault planes suggest dextral strike-slip patterns with an oblique component towards N82E.

$^{40}Ar/^{39}Ar$ DATING OF MUSCOVITE

$^{40}Ar/^{39}Ar$ dating was undertaken for coarse-grained muscovite crystals collected along two N30E fault planes 140 kilometers apart. In both cases the rock faulted is granite. One of the points (PTZ-01) is situated south of Brasil Novo (52°33'19"W / 3°37'39"S). The age of 1977 ± 8 Ma is defined by both ideogram peak and plateau (Figs. 5a and 5b; Tab. 1).

Another studied outcrop (PMI-19) is located near Anapu (51°13'31"W/3°26'47"S). The age defined by the plateau is 1975 ± 9 Ma, within error of the age of 1968 ± 11 Ma obtained by the ideogram peak (Figs. 5c and5d; Table 1).The similar ages obtained by ideogram peaks and plateau indicate on one hand that the ages are real and on the other hand that the ideograms represent have high probability peaks. The similarity of the ages obtained from the outcrops suggests that this phase

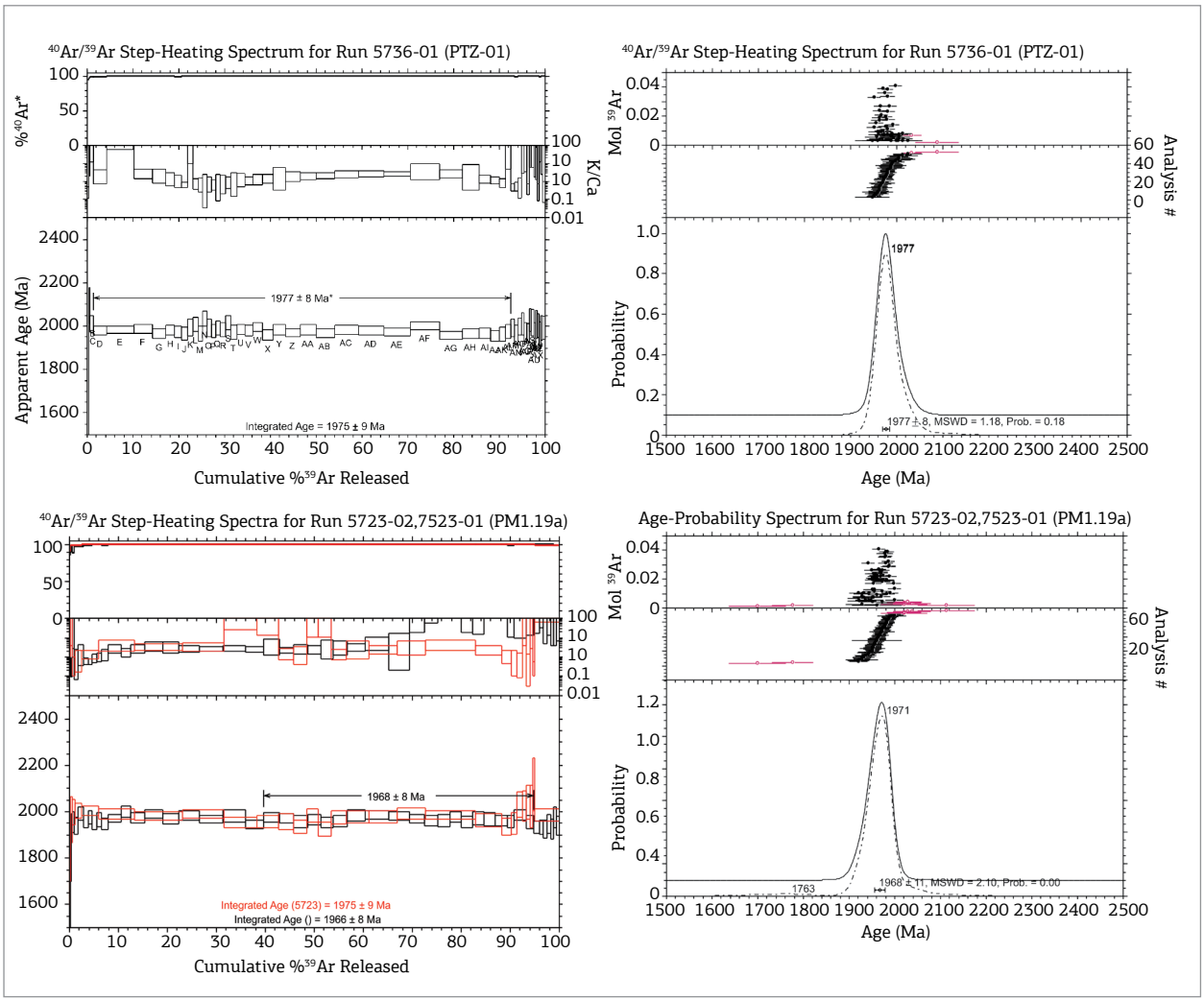

Figure 5. Diagrams of $^{40}Ar/^{39}Ar$ dating of muscovite collected on fault planes affecting Paleoproterozoic granites from Bacajá Terrane, Pará state. (A)and (B) Plateau and ideogram from the sample PTZ-01; (C) and (D) Plateau and ideogram from the sample PMI-19. Sample locations are shown in Fig. 2.

Table 1. Ar-Ar analyses of muscovite from brittle faults that crosscut Paleoproterozoic granites, Bacajá terrane.

Run ID	Sample	$^{37}Ar/^{39}Ar$	$^{38}Ar/^{39}Ar$	$^{40}Ar/^{39}Ar$	$^{40}Ar^*/^{39}Ar$	$\%^{40}Ar^*$	Age Ma
5723-01A	PMI-19a	1.4	0.0211	468	429	91.56	1702
5723-01B	PMI-19a	0.54	0.0187	545	538	98.66	1962
5723-01C	PMI-19a	0.98	0.0113	559	553	98.79	1995
5723-01D	PMI-19a	0.47	0.0104	558.3	555.4	99.45	2000
5723-01E	PMI-19a	0.372	0.0132	557.4	555.8	99.69	2001
5723-01F	PMI-19a	0.117	0.009	551.1	549.9	99.773	1988
5723-01G	PMI-19a	0.157	0.01186	547	545.8	99.768	1979.3
5723-01I	PMI-19a	0.141	0.0115	550.3	549.5	99.832	1987.3
5723-01J	PMI-19a	0.054	0.011	534.5	533.3	99.77	1951
5723-01K	PMI-19a	0.096	0.0096	535.8	534.7	99.79	1955
5723-01L	PMI-19a	0.309	0.0086	536.7	535.3	99.72	1956
5723-01M	PMI-19a	0.27	0.0112	527	525.5	99.7	1934
5723-01N	PMI-19a	0.14	0.0133	548.9	547.5	99.73	1983
5723-01O	PMI-19a	0.126	0.0077	521.3	520.2	99.77	1922
5723-01P	PMI-19a	0.354	0.0106	544.5	543.6	99.82	1974
5723-01Q	PMI-19a	0.147	0.0101	544.2	543.5	99.85	1974
5723-01R	PMI-19a	0.202	0.0111	545.1	544.4	99.872	1976
5723-01S	PMI-19a	0.138	0.01276	551.6	550.6	99.8	1990
5723-01T	PMI-19a	0.112	0.01392	548.4	547.2	99.78	1982.4
5723-01U	PMI-19a	0.217	0.0118	539.8	538.6	99.77	1963
5723-01V	PMI-19a	0.4	0.0113	525.8	525.3	99.87	1933
5723-01W	PMI-19a	0.47	0.0099	533	532	99.68	1948
5723-01X	PMI-19a	0.63	0.0148	570	569	99.68	2029
5723-01Y	PMI-19a	0.38	0.0056	567	566	99.85	2023
5723-01Z	PMI-19a	0.79	0.018	575	573	99.59	2039
5723-01AA	PMI-19a	0.54	0.004	566	565	99.9	2022
5723-01AB	PMI-19a	1.62	0.0076	611	610	99.75	2115
5723-01AC	PMI-19a	0.035	0.0136	550.8	547.8	99.45	1984
5723-02A	PMI-19a	1.96	0.0692	257	133.3	51.8	716
5723-02B	PMI-19a	2.4	0.051	360	314	87.1	1380
5723-02C	PMI-19a	2.35	0.0554	510	459	89.83	1777
5723-02D	PMI-19a	1.12	0.0203	538	524	97.29	1930
5723-02E	PMI-19a	0.45	0.0449	600	534	88.95	1953
5723-02F	PMI-19a	0.43	0.0218	539.7	526.7	97.56	1937
5723-02G	PMI-19a	0.233	0.0131	562.9	551	97.86	1991
5723-02H	PMI-19a	0.85	0.0161	537.6	534.9	99.45	1955
5723-02I	PMI-19a	0.92	0.0181	548.6	542.6	98.85	1972
5723-02J	PMI-19a	0.55	0.0128	535.2	533.7	99.68	1952
5723-02K	PMI-19a	0.51	0.0162	539.7	538.7	99.776	1963
5723-02L	PMI-19a	0.37	0.0176	532.2	530.1	99.58	1944
5723-02M	PMI-19a	0.189	0.0115	542.8	541.5	99.74	1969.7
5723-02N*	PMI-19a	0.274	0.01127	555.5	554.6	99.82	1999
5723-02O	PMI-19a	0.178	0.01326	543.6	542.4	99.77	1972

Continue...

Table 1. Continuation.

Run ID	Sample	$^{37}Ar/^{39}Ar$	$^{38}Ar/^{39}Ar$	$^{40}Ar/^{39}Ar$	$^{40}Ar^*/^{39}Ar$	$\%^{40}Ar^*$	Age Ma
5723-02Q	PMI-19a	0.135	0.01057	550.9	550.1	99.85	1988.8
5723-02R	PMI-19a	0.146	0.01443	541.8	540.4	99.736	1967
5723-02S	PMI-19a	0.192	0.0122	547.9	546.8	99.794	1981
5723-02T	PMI-19a	0.196	0.00826	541.4	540.3	99.798	1967.2
5723-02U	PMI-19a	0.178	0.01214	547.2	546.4	99.86	1981
5723-02V	PMI-19a	0.202	0.01095	530.5	530	99.9	1944.1
5723-02W	PMI-19a	0.112	0.01173	545.1	543.8	99.76	1975
5723-02X	PMI-19a	0.228	0.01107	543.5	542.1	99.72	1971
5723-02Y	PMI-19a	0.182	0.0098	536.6	535.2	99.73	1956
5723-02Z	PMI-19a	0.204	0.0119	539.2	538.1	99.78	1962
5723-02AA	PMI-19a	0.13	0.0139	534.7	533.5	99.772	1952
5723-02AB	PMI-19a	0.135	0.0109	537.3	536.1	99.77	1958
5723-02AC	PMI-19a	0.161	0.01278	548.1	546.8	99.76	1982
5723-02AD	PMI-19a	0.084	0.0137	550	548.6	99.75	1985.4
5723-02AF	PMI-19a	0.062	0.01226	546.9	546.3	99.881	1980.3
5723-02AG	PMI-19a	0.064	0.00837	541.7	540.7	99.82	1968
5723-02AH	PMI-19a	0.036	0.0112	537.6	536.7	99.83	1959
5723-02AI	PMI-19a	0.015	0.0135	538.2	537.2	99.82	1960
5723-02AJ	PMI-19a	0.029	0.0086	545.1	544.3	99.85	1976
5723-02AK	PMI-19a	0.074	0.0108	534.7	533.5	99.78	1952
5723-02AL	PMI-19a	0.083	0.0124	542.3	541.4	99.82	1970
5723-02AM	PMI-19a	0.008	0.0121	540.6	539.3	99.764	1965
5723-02AN	PMI-19a	0.001	0.0126	537.6	536.5	99.8	1959
5723-02AO	PMI-19a	0.13	0.0165	537.6	535.4	99.58	1956
5723-02AR	PMI-19a	0.124	0.00922	549.1	547.9	99.78	1984
5723-02AS	PMI-19a	0.12	0.0118	535.3	534.2	99.774	1953
5723-02AT	PMI-19a	0.12	0.0124	525.1	523.8	99.76	1930
5723-02AU	PMI-19a	0.09	0.0112	523.8	523.8	100	1930
5723-02AV	PMI-19a	0.28	0.014	521.4	520.4	99.8	1922
5723-02AW	PMI-19a	0.18	0.0141	531.9	530.6	99.75	1946
5723-02AX	PMI-19a	0.34	0.011	523.1	520.7	99.53	1923
5723-02AY	PMI-19a	0.37	0.0068	547	543	99.35	1974
5723-02AZ	PMI-19a	0.25	0.0201	531.6	527.1	99.13	1937
5736-01A	PTZ-01	1.73	0.0124	182.6	173.2	94.73	886
5736-01B	PTZ-01	0.9	0.0319	615	597	97.08	2090
5736-01C	PTZ-01	0.18	0.0133	563.6	558	98.99	2007
5736-01D	PTZ-01	0.22	0.01234	546.8	544.4	99.54	1977
5736-01E	PTZ-01	0.029	0.01227	547.3	546.4	99.83	1981.4
5736-01F	PTZ-01	0.172	0.01179	549.1	548.4	99.864	1986
5736-01G	PTZ-01	0.184	0.0103	539.4	538.4	99.82	1964
5736-01H	PTZ-01	0.294	0.0125	546.3	546	99.91	1981
5736-01I	PTZ-01	0.4	0.0116	543.5	541.9	99.67	1972
5736-01J	PTZ-01	0.8	0.0122	538.9	538.4	99.85	1964

Continue...

Table 1. Continuation.

Run ID	Sample	$^{37}Ar/^{39}Ar$	$^{38}Ar/^{39}Ar$	$^{40}Ar/^{39}Ar$	$^{40}Ar^*/^{39}Ar$	$\%^{40}Ar^*$	Age Ma
5736-01K	PTZ-01	0.17	0.0117	551.7	550.5	99.77	1990
5736-01L	PTZ-01	0.64	0.0099	559.2	558.1	99.75	2007
5736-01M	PTZ-01	0.57	0.012	539.4	537.5	99.62	1962
5736-01N	PTZ-01	0.44	0.0089	571.8	570.5	99.75	2034
5736-01O	PTZ-01	0.53	0.014	550.4	549.8	99.86	1989
5736-01P	PTZ-01	0.7	0.0125	544.7	543.2	99.68	1975
5736-01Q	PTZ-01	0.4	0.014	551.9	550.5	99.72	1991
5736-01R	PTZ-01	0.43	0.0058	546.4	546.4	99.97	1982
5736-01S	PTZ-01	0.5	0.0116	562	561.4	99.86	2014
5736-01T	PTZ-01	0.34	0.0173	541.8	540.6	99.76	1969
5736-01U	PTZ-01	0.33	0.0143	548	546.8	99.76	1982
5736-01V	PTZ-01	0.45	0.0115	545.6	544.4	99.75	1977
5736-01W	PTZ-01	0.336	0.0109	552	551.5	99.89	1993
5736-01X	PTZ-01	0.338	0.0121	536.5	535.3	99.75	1957
5736-01Y	PTZ-01	0.161	0.0109	546.6	546	99.872	1981
5736-01Z	PTZ-01	0.24	0.008	541.2	540.3	99.82	1968
5736-01AA	PTZ-01	0.241	0.0118	547.5	546.6	99.809	1982
5736-01AB	PTZ-01	0.239	0.0117	540.9	539.6	99.76	1966.6
5736-01AC	PTZ-01	0.208	0.00969	548.1	546.9	99.75	1983
5736-01AD	PTZ-01	0.192	0.0142	545.2	544.1	99.8	1977
5736-01AE	PTZ-01	0.197	0.0128	542.8	541.8	99.788	1971.3
5736-01AF	PTZ-01	0.099	0.0096	555.4	554.4	99.8	1999
5736-01AG	PTZ-01	0.183	0.01161	534.9	533.9	99.79	1953.8
5736-01AH	PTZ-01	0.129	0.01132	539.3	538.3	99.81	1964
5736-01AI	PTZ-01	0.345	0.0126	540.4	539.1	99.73	1965
5736-01AJ	PTZ-01	0.458	0.0171	534.7	533.4	99.73	1953
5736-01AK	PTZ-01	0.6	0.0123	538.1	536.9	99.73	1960
5736-01AL	PTZ-01	0.27	0.0124	544.4	542.9	99.72	1974
5736-01AM	PTZ-01	1.05	0.0113	551.6	549.8	99.62	1989
5736-01AN	PTZ-01	0.91	0.0168	538.4	535.9	99.48	1958
5736-01AO	PTZ-01	0.63	0.0113	554.3	553	99.73	1996
5736-01AP	PTZ-01	0.51	0.0103	559	558	99.82	2007
5736-01AQ	PTZ-01	0.42	0.0068	543	541	99.72	1970
5736-01AR	PTZ-01	1.19	0.0111	540	539	99.78	1965
5736-01AS	PTZ-01	0.31	0.0117	569	567	99.61	2026
5736-01AT	PTZ-01	0.34	0.0056	563	561	99.69	2014
5736-01AU	PTZ-01	0.74	0.0026	534	532	99.59	1950
5736-01AV	PTZ-01	0.86	0.0155	559	557	99.65	2005
5736-01AW	PTZ-01	1.32	0.0126	557	555	99.58	2000
5736-01AX	PTZ-01	0.23	0.0159	540	537	99.42	1961
5736-01AY	PTZ-01	0.58	0.0075	550	550	99.94	1990
5736-01AZ	PTZ-01	1	0.0048	552	550	99.53	1989

of deformation took place on a regional scale. During the Transamazonian Cycle, the voluminous syntectonic granite magmatism that marked the evolution of the Bacajá recorded different moments of compressive stress during crystallization and emplacement of granite bodies. These late structures have taken place in the orogeny evolution at lower temperatures than those of the mylonites (which formed under temperatures higher than 400ºC).

Alike studies correlating structural data of granites and $^{40}Ar/^{39}Ar$ ages were realized in Late Ordovician units from the Caledonian orogen in Norway (Scheiber *et al*. 2016) and in the Eocene Adamello massif, Italian Alps (Pennacchione *et al*. 2006). In both cases brittle structures are related to the final compressional stress that played a role close to the magmatic cooling.

DISCUSSION

During the emplacement of the granite plutons in the Bacajaí, Arapari and João Jorge intrusive suites, magmatic structures (igneous layering and magmatic foliation with solid state components) developed throughout the region. These structures reflect deformation during emplacement and early crystallization of the granite bodies. At this stage, inflation of magma chambers may have enhanced flow and differentiation, resulting in igneous layering.

In the Paleoproterozoic domains of the West African craton Pons *et al*. (2006) considered most of the structures in the granites to be developed by the mixing of heterogeneous magmas and the movement of crystals and liquids via thermal convection. Pons *et al*. (2006) also admitted that the segregation of magmas within their chambers were mechanisms responsible for igneous layering. These processes most probably had an impact on the felsic to intermediate magmas of the Bacajá Terrane. According to Pons *et al*. (2006), the close association of igneous layering with the existence of mafic enclaves in calc-alkaline plutons suggests that the layering formed due to recurrent injection of basic magmas. In this case, disruption and mixing of the mafic enclaves with acid to intermediate magma may be the effective cause of the development of layering. However, layering of igneous rocks may form by a number of mechanisms, and disruption of early-formed enclaves is just one of them in the granites from the Bacajá region.

With the significant changes that occur in the liquid/crystal ratio during crystallization (Vigneresse *et al*. 1996, Barbey 2009), regional structural behavior of the granitoids in the Bacajá Terrane and widespread magmatic foliation would have been formed during crystallization. These submagmatic structures are recorded by the homogenous preferred orientation of minerals at a regional scale, the scale of outcrops and in thin section. The flattening of quartz crystals commonly found in syntectonic granites (Gapais & Barbarin 1986) is a clear example of magma deformation reaching the rheological threshold. These structures could be formed under conditions of decreasing temperatures and increasing strain rates, as expected in syntectonic granites.

In the Transamazonas Province, the different pulses of granite emplacement in a compressive tectonic stress field are evidenced by the elongated form of the intrusions on aeroradiometric maps (Carneiro *et al*. 2012). The elongated shapes of the syntectonic granites, their contacts with host rocks, and/or their different rheology, together with their fabric would have resulted in domains of contrasting rheology and structural anisotropy. In the study area some ductile shear zones, phyllonitic shear zones and faults developed along boundaries between granite plutons or along contact between petrographic facies. Cross-cutting relations and differences in thermal regime show that the ductile-brittle (phyllonites) and brittle-ductile shear zones (cataclasites) formed after the regional ductile foliation in the granites.

Other ductile shear zone controlled by rheological differences is found located to the northeast and south of Anapu, along the contacts between the granites of the Arapari and Bacajá Paleoproterozoic suites and the Neoarchean orthogneisses of the Aruanã complex. The Neoarchean domain probably behaved more rigidly and deformation there would have been more easily accommodated by the Paleoproterozoic granitoids of domains characterized by higher thermal gradients.

According to Ranalli (2000), preexisting faults can be reactivated if the difference of necessary stress is lower than the difference of critical stress for the formation of a new shear plane where tectonic stress is high. Weak zones (Holdsworth *et al*. 1997) may be represented by such structural anisotropies as shear zones, faults and rheological discontinuities. These anisotropies are locations that enhance tectonic reactivation. The Bacajá domain contains the first two of the four types of criteria used by Holdsworth *et al*. (1997) to identify reactivation features (structural, geochronological and stratigraphic).

CONCLUSIONS

The syntectonic granites of the Transamazonas province exhibit structures formed under different temperature and rheological conditions. In the initial phases of pluton evolution, igneous layering was controlled by the dynamics of the magmatic chambers and by regional compressive forces, so that deformation would have occurred in not

completely crystallized magma. Under these conditions, most deformation is recorded by regional homogenous subhorizontal shortening. With a decrease in temperature, recrystallization would have increased, along with the progressive development of submagmatic foliation. The subsequent evolution from ductile, ductile-brittle, brittle-ductile shear zones, and eventually brittle faults testifies to deformation during a period of cooling. The geochronological data available for the Bacajá region point to a protracted history of construction of magmatic arcs from 2200 Ma to 2080 Ma. $^{40}Ar/^{39}Ar$ ages obtained on muscovite from brittle strike/slip faults (N33E/87SE) suggest that the brittle conditions were reached at ~1975 Ma, about 100 m.y. after the emplacement of the Arapari (2150 Ma) and João-Jorge (2075 Ma) granite suites. Structural observations suggest that compressive forces persisted during this time interval. Hence it seems that in long duration Paleoproterozoic orogenetic zones, the installation of successive magmatic arcs was associated with stresses that were maintained for a long time after the complete crystallization of the arc-related plutons. The Paleoproterozoic brittle faults present in granites from the Bacajá Terrane are rare examples of preserved old structures that were not reactivated by younger deformation.

ACKNOWLEDGEMENTS

The authors would like to thank to Petrobras and the Geology Department from the Universidade Federal do Paraná (UFPR) for their financial and institutional support. We are grateful to the referees for the precious critics and suggestion and to the editors for the valuable opportunity. We would like to thank to Haakon Fossen for valuable editorial help. E. Perico thanks the Geology post-graduation program from the UFPR. C.E.M. Barros is grateful to the Conselho Nacional de Desenvolvimento Científico e Tecnológico (CNPq) by the research support (Grants 306468/2009–3 and 309625/2015-7).

REFERENCES

Arzi A.A. 1978. Critical phenomena in the rheology of partially melted rocks. *Tectonophysics,* **44**:173-184.

Avelar V.G., Lafon J.M., Delor C., Guerrot C., Lahondère D. 2003. Archean crustal remnants in the easternmost part of the Guiana Shield: Pb–Pb and Sm–Nd geochronological evidence for Mesoarchean versus Neoarchean signatures. *Géologie de la France,* **2-3-4**:83-100.

Bailey W. R., Walsh J. J., Manzocchi T. 2005. Fault populations, strain distribution and basement fault reactivation in the East Pennines Coalfield, UK. *Journal of Structural Geology,* **27**:913-928.

Barbey P. 2009. Layering and schlieren in granitoids: a record of interactions between magma emplacement, crystallization and deformation in growing plutons. *Geologica Belgica,* **12**(3-4):109-133.

Barbey P., Gasquet D., Pin C., Bourgeix A.-L., 2008. Igneous banding, schlieren and mafic enclaves in calc-alkaline granites: The Budduso pluton (Sardinia). *Lithos,* **104**:147-163.

Barros C.E.M., Barbey P., Boullier A.M. 2001. Role of magma pressure, tectonic stress and crystallization progress in the emplacement of the syntectonic A-type Estrela Granite Complex (Carajás Mineral Province, Brazil). *Tectonophysics,* **343**:93-109.

Barros C.E.M., Macambira M.J.B., Santos M.C.C., Silva D.C.C., Palmeira L.C., Sousa M.M. 2007. Estruturas sin-magmáticas e idade Pb-Pb em zircão (evaporação) de granitos paleoproterozoicos da Província Maroni-Itacaiúnas. *Revista Brasileira de Geociências,* **37**:293-304.

Brown D., Alvarez-Marron J., Perez-Estaun A., Puchkov V., Ayala C. 1999. Basement influence on foreland thrust and fold belt development: an example from the southern Urals. *Tectonophysics,* **308**:459-472.

Bumby A.J., Eriksson P.G., Van Der Merwe R., Brümmer J.J. 2001. Shear-zone controlled basins in the Blouberg area, Northern Province, South Africa: syn- and post-tectonic sedimentation relating to ca. 2.0 Ga reactivation of the Limpopo Belt. *Journal of Structural Geology,* **33**:445-461.

Carneiro C.C., Fraser S.J., Crosta A.P., Silva A.M., Barros C.E.M. 2012. Semiautomated geologic mapping using self-organizing maps and airborne geophysics in the Brazilian Amazon.*Geophysics,* **77**:17-24.

Cordani U.G., Fraga L.M., Reis N., Tassinari C.C.G., Brito-Neves B.B. 2010. On the origin and tectonic significance of the intra-plate events of Grenvillian-type age in South America: A discussion. *Journal of South American Earth Sciences,* **29**(1):143-159.

Cordani U.G., Tassinari C.C.G., Teixeira W., Basei M.A.S., KawashitaK. 1979. Evolução tectônica da Amazônia com base nos dados geocronológicos. *In*: Congresso Geológico Chileno, 2., 1979. *Actas*... Arica, Chile, p. 137-148.

Corrêa-Gomes L.C., Dominguez J.M.L., Barbosa J.S.F., Silva I.C. 2005. Padrões de orientação dos campos de tensão, estruturas, herança do embasamento e evolução tectônica das bacias de Camamú e porção sul do Recôncavo, Costa do Dendê, Bahia. *Revista Brasileira de Geociências,* **35**:117-128.

Delor C., Lahondère D., Egal E., Lafon J.M., Cocherie A., Guerrot C., Rossi P., Truffert C., Théveniaut H., Phillips D., Avelar V.G. 2003. Transamazonian crustal growth and reworking as revealed by the 1:500,000–scale geological map of French Guiana (2nd edition). *Géologie de la France,***2-3-4**:5-57.

Faraco M.T.L., Vale A.G., Santos J.O.S., Luzardo R., Ferreira A.L., Oliveira M., Marinho P.A.C. 2005. Levantamento geológico da região ao norte da Província Carajás. *In*: Horbe A.M.C. & Souza V.S. (eds.). *Contribuições à Geologia da Amazônia*. Manaus: SBG, p. 16-31.

Gapais D. & Barbarin B. 1986. Quartz fabric transition in a cooling syntectonic granite (Hermitage Massif, France). *Tectonophysics,* **125**:357-370.

Gower C.F. 1993. Syntectonic minor intrusions or synemplacement deformation? *Canadian Journal of Earth Sciences,* **30**:1674-1675.

Holdsworth R.E., Butler C.A., Roberts A.M. 1997. The recognition of reactivation during continental deformation. *Journal of the Geological Society of London,* **154**:73-78.

João X.S.J., Vale A.G., Lobato T.A.M. 1987. *Projeto especial mapas de recursos minerais de solos e de vegetação para a área do programa Grande Carajás; Subprojeto Recursos Minerais, Folha SA.22-Y-D,Altamira*. Brasília: DNPM/CPRM. 31 p.

Korme T., Acocella V., Abebe B. 2004. The Role of Pre-existing Structures in the Origin, Propagation and Architecture of Faults in the Main Ethiopian Rift. *Gondwana Research,* **7**:467-479.

Lima M.I.C., Penalber L.O.G., Coelho F.A.J.F., Bezerra P.E.L. 2005. Esboço tectônico da Folha SB.22X-A (Novo Repartimento) (PA). *In*: Simpósio de Estudos Tectônicos, 10. *Boletim de resumos expandidos*. SBG, p. 322-324.

Macambira M.J.B., Vasquez M.L., Silva D.C.C., Galarza M.A., Barros C.E.M., Camelo J.F. 2009. Crustal growth of the central-eastern Paleoproterozoic domain, SE Amazonian craton: Juvenile accretion vs. reworking. *Journal of South American Earth Sciences,* **27**:235-246.

Mansy J.L., Manby G.M., Averbuch O., Everaerts M., Bergerat F., Van Vliet-Lanoe B., Lamarche J.,Vandycke S. 2003. Dynamics and inversion of the Mesozoic Basin of the Weald–Boulonnais area: role of basement reactivation. *Tectonophysics,* **373**:161-179.

Marshak S., Alkmim F.F., Whittington A., Pedrosa-Soares A.C. 2006. Extensional collapse in the Neoproterozoic Araçuaí orogen, eastern Brazil: a setting for reactivation of asymmetric crenulation cleavage. *Journal of Structural Geology,* **28**:129-147.

Miller R.B. & Paterson S.R. 1994. The transition from magmatic to high-temperature solid-state deformation implications from the Mount Stuart Batholith, Washington. *Journal of Structural Geology,* **16**:853-865.

Paterson S.R., Fowler Jr., T.K., Schmidt K.L., Yoshinobu A.S., Yuan E.S., Miller R.B. 1998. Interpreting magmatic fabric patterns in plutons. *Lithos,* **44**:53-82.

Paterson S.R., Vernon R.H., Fowler Jr. T.K. 1991. Aureole systematics. *In*: Ribbe, P.H. *Contact Metamorphism, Reviews in Mineralogy,* **26**:673-722.

Paterson S.R., Vernon R.H., Tobisch O.T. 1989. A review of criteria for the identification of magmatic and tectonic foliations in granitoids. *Journal of Structural Geology,* **11**:349-363.

Pawley M.J. & Collins W.J. 2002. The development of contrasting structures during the cooling and crystallization of a syn-kinematic pluton. *Journal of Structural Geology,* **24**:469-483.

Pennacchione G., Di Toro G., Brack P., Menegon L., Villa I.M. 2006. Brittle-ductile-brittle deformation during cooling of tonalite (Adamello, Southern Italian Alpes). *Tectonophysics,* **427**:171-197.

Perico E. 2010. *Análise estrutural da Província Maroni-Itacaiúnas e da Bacia do Amazonas na região de Altamira (PA)*. MS Dissertation, Universidade Federal do Paraná, Curitiba, 122 p.

Pinheiro R.V.L. & Holdsworth R.E. 1997. Reactivation of Archean strike-slip fault system, Amazon region, Brazil. *Journal of the Geological Society of London,* **154**:99-103.

Pons J., Barbey P., Dupuis, D., Léger, J.M. 1995. Mechanism of pluton emplacement and structural evolution of a 2.1 Ga juvenile continental crust: The Birimian of southwestern Niger. *Precambrian Research,* **70**:281-301.

Pons J., Barbey P., Nachit H., Burg J.P. 2006. Development of igneous layering during growth of plutons: the Tarçouate Laccolith (Morocco). *Tectonophysics,* **413**:271-286.

Ranalli G. 2000. Rheology of the crust and its role in tectonic reactivation. *Journal of Geodynamics,* **30**:3-15.

Rosa-Costa L.T., Lafon J.M., Delor C. 2006. Zircon geochronology and Sm-Nd isotopic study: further constraints for Archean and Paleoproterozoic geodynamical evolution of the southeastern Guiana Shield, north of Amazonian craton, Brazil. *Gondwana Research,* **10**:277-300.

Rostirolla S.P., Mancini F., Rigoti A., Kraft R.P. 2001. Structural styles of the intracratonic reactivation of the Perimbó fault zone, Paraná basin, Brazil. *Journal of South American Earth Sciences,* **16**:287-300.

Santos J.O.S. 2003. Geotectônica dos Escudos da Guiana e Brasil Central. *In*: Bizzi L.A.; Schobbenhaus C.,Vidotti R.M., Gonçalves J.H. (eds.). *Geologia, tectônica e recursos Minerais do Brasil*. Texto, mapas e SIG. CPRM-Serviço Geológico do Brasil, **4**:169-226.

Santos J.O.S., Hartmann L.A., Gaudette H.E., Groves D.I., Mcnaughton N.J., FlecherI.R. 2000. A new understanding of the Amazon Craton provinces, based on field work and radiogenic isotope data. *Gondwana Research,* **3**:453-488.

Scheiber T., Viola G., Wilkinson C.M., Ganerod M., Skar O., Gasser D. 2016. Direct $^{40}Ar/^{39}Ar$ dating of Late Ordovician and Silurian brittle faulting in the southwestern Norwegian Caledonides. *Terra Nova,* **28**(5):374-382.

Tassinari C.C.G. & Macambira M.J.B. 2004. A evolução tectônica do Cráton Amazônico. *In*: Mantesso-Neto V., Bartorelli A., Carneiro C.D.R., Brito-Neves B.B. *Geologia do Continente Sul-Americano: Evolução da Obra de Fernando Flávio Marques de Almeida*. São Paulo: Beca. p.471-485.

Vasquez M.L., Macambira M.J.B., Armstrong R.A. 2008. Zircon geochronology of granitoids from the western Bacajá domain, southeastern Amazonian craton, Brazil: Neoarchean to Orosirian evolution. *Precambrian Research,* **161**:279-302.

Vasquez M.L., Macambira M.J.B., Galarza M.A. 2005. Granitóides transamazônicos da região Iriri-Xingu, Estado do Pará: novos dados geológicos e geocronológicos. *In*: Horbe A.M.C. & Souza V.S. (eds.). *Contribuições à Geologia da Amazônia*. Manaus: SBG, **4**:16-31.

Vasquez M.L. & Rosa-Costa L.T. 2008. *Geologia e recursos minerais do Estado do Pará:* Sistema de Informações Geográficas SIG: texto explicativo dos mapas Geológico e de Recursos Minerais do Estado do Pará (escala 1:1.000.000). Belém, CPRM, 328 p.

Vauchez A., Tommasi A., Barruol G. 1998. Rheological heterogeneity, mechanical anisotropy and deformation of the continental lithosphere. *Tectonophysics,* **296**:61-86.

Vigneresse J.L., Barbey P., Cuney M. 1996. Rheological transitions during partial melting and crystallization with application to felsic magma segregations and transfer. *Journal of Petrology,* **37**:1579-1600.